2016 IEEE/RSJ International Conference on Intelligent Robots and Systems (IROS)
Daejeon Convention Center
October 9-14, 2016, Daejeon, Korea

Design of a Multilink-articulated Wheeled Inspection Robot for Winding Pipelines: AIRo-II

Atsushi Kakogawa[1] and Shugen Ma[2]

Abstract— **This paper presents a multilink-articulated robot with omni and hemispherical wheels (AIRo-II) for inspecting and exploring winding pipes. To quickly adapt to winding pipes, holonomic rolling movement without moving forward and backward is more useful. However, this requires the replacement of driving actuators with rolling actuators at the expense of the driving force. In this paper, we investigate the possibility of high maneuverability of multilink-articulated robots in winding pipes by using less actuators and by designing spring joints. We further validate this by experimental verification.**

I. INTRODUCTION

Identifying deterioration points in aging pipelines is a very important task to avoid critical leakage and explosion accidents. Till date, researchers and engineers have tried developing inspection robots to look inside narrow pipes where humans cannot enter. The risk of accessing the pipelines, especially those placed underground or at high places, can be avoided if the pipes can be inspected from the inside by robots instead of humans.

Recently, highly adaptable in-pipe inspection robots that resemble railway trains and redundant manipulators have been developed. These robots, which are often called snake-like robots, possess rope-like bodies. They are capable of superior performances especially in the bend and branch of pipes due to their rope-like bodies.

Multi-segmented and cable-free robot platforms, namely the "MAKRO and KAIRO series" are developed by INSPECTOR SYSTEMS, Rainer Hitzel GmbH, Germany [1]–[3]. These robots wriggle using oblique joints. They also develop another type of multi-segmented inspection robot called "INSPECTOR" that adapts to vertical pipes. For a while, Schempf et al. have focused on the "Explore" project for inspecting live gas mains [4]. This robot system is untethered, self-powered, and wirelessly controlled. Recently, the Explore project has been put to practical use by Pipetel Technologies Inc. Choi et al. are advancing the MRINSPECT project for inspection of gas pipelines. The latest robot, called "MRINSPECT VII," is equipped with differential mechanisms, and the joints between the segments are backdrivable [5], [6]. INSPECTOR, Explore and MRINSPECT VII can press against the inner wall of the pipe with expandable active arm mechanisms and can go up the vertical pipes.

*This work was supported by Nippon Venture Capital Co., Japan and The Japan Science and Technology Agency (JST).

[1]Atsushi Kakogawa is with Department of Robotics, Faculty of Science and Engineering, Ritsumeikan University, 1-1-1, Noji-higashi, Kusatsu, Shiga, Japan kakogawa@fc.ritsumei.ac.jp

[2]Shugen Ma is with Department of Robotics, Faculty of Science and Engineering, Ritsumeikan University, 1-1-1, Noji-higashi, Kusatsu, Shiga, Japan shugen@se.ritsumei.ac.jp

TABLE I
EXISTING MULTILINK-ARTICULATED WHEELED ROBOTS

Clamping type	Robot	Joint type	Diameter [mm]
N/A	MAKRO & KAIRO	A-O	250
Expandable arm	INSPECTOR	P-P & P-Y (Flexible)	75-750
	Explore	A-P & A-Y	150-200
	MRINSPECT VII	A-P & A-Y	150-200
Body-bending	PIRATE	A-P & A-R	75
	PIPETRON-I	A-P &A-Y (Tendon)	75
	PIPETRON-II	P-P & A-Y	75
	PiKo	A-P & A-Y	250

A-O: Active oblique, A-R: Active roll, P-P: Passive pitch, A-P: Active pitch, P-Y: Passive yaw, A-Y: Active yaw

Dertien et al. designed a multilink-articulated wheeled robot called "PIRATE." Its joints are actuated by motor and torsion springs that clamp the robot in the pipe [7], [8]. Another active joint placed at the center of the robot could twist half of the body to change the steering direction. A different version of the PIRATE series with omni wheels was also reported. It possessed a joint that was passively bent in the pipe by the rubber band that connected the links. Hirose et al. proposed the "PIPETRON series" (also called "THES" in some literature), which also adopted the multilink-articulated wheeled mechanism [9], [10]. In the PIPETRON-I, two wires were distributed to bend each joint in the pitch and yaw directions. A wire caused the robot's wheel to touch the pipe wall. Another wire twists the robot's body to helically move it in the straight pipe by aligning the steering direction of the robot beforehand. The PIPETRON-II was developed as the second generation of the PIPETRON series. It maintained the zigzag shape of the robot using torsion springs mounted at the joints. The latest version of the PIPETRON was also reported. However, due to contractual reasons, concrete information has not been published yet. Transeth et al. proposed a snake-like inspection robot called "PiKo." The use of the pitch and yaw active joints allowed the robot to steer itself. They also clamped the robot's body in the pipe [11]. The robots have no expandable arm mechanisms. Instead, they press against the inner wall of the pipe by bending their own bodies, like an inchworm.

Among the robots, the former and latter types can be categorized as expandable-arm- and body-bending-types, respectively as listed in Table I. If the space to mount the expandable arm mechanisms is not sufficient, body bending is more feasible for downsizing. Looking back the history of

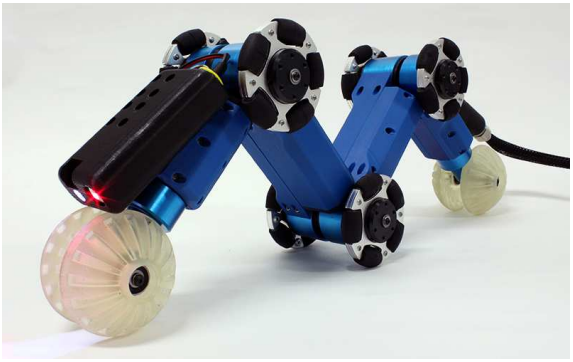

Fig. 1. Overview of the AIRo-II

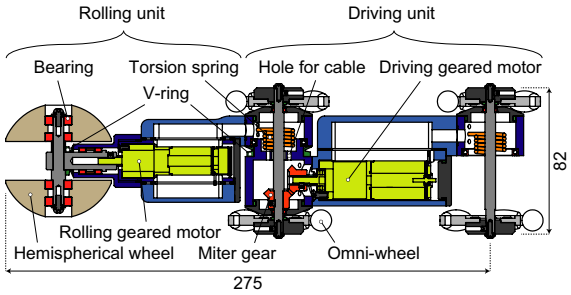

Fig. 2. Cross-sectional view of the half of the robot

TABLE II
SPECIFICATION OF THE AIRO-II

Adaptive diameter [m]	0.1
Total length (when extended) [m]	0.55
Total weight [kg]	1.7
Maximum traction force [kgf]	4.0
Maximum speed [m/s]	0.3

the in-pipe inspection robots, the body bending type named "Pipemouse" was proposed by Foster-miller Inc. in 2004 [12], and its prototype appeared in [4]. Most of the body-bending-type robots steer at the bend and branch pipes by three-dimensionally swinging the links or helically moving around the pipe axis. However, to quickly align the steering direction, holonomic rolling movement that eliminates forward and backward movements in the pipe is more useful, especially in the short and winding pipe. The articulated robot that uses omni wheels and can holonomically roll was also reported before [8]. However, due to their small radii, small passive wheels that surrounded the omni wheel were not adaptable in the traveling direction. To solve this shortcoming, we designed a multilink-**A**rticulated **I**nspection **Ro**bot with omni and hemispherical wheels (AIRo-II) as shown in Fig. 1. Omnidirectional mobile robots that combine the hemispherical wheels achieve a high obstacle adaptability in all planar directions [13]–[15]. Inspired by this, the first generation of our pipeline inspection robot was introduced in [16]. A pair of the hemispherical wheels was attached at the end of the robot. They freely rotated in the traveling direction and driven around the link axis by a motor. Although, this robot was not yet adaptable to the circumferential direction of the pipe, it could avoid obstacles by moving forward and backward.

For the holonomic rolling movement in the pipe, it was necessary to replace driving actuators with rolling actuators at the expense of the driving force. In our case, there were four housings that could be mounted on the actuators; however, two of the housings must be replaced with rolling actuators. Additionally, if the joint actuation could be replaced by the torsion spring, both the total weight and the cost of the robot could be reduced. Thus, maintenance becomes easier. Therefore, in this paper, we pursue the possibility of achieving high maneuverability in the winding pipes with only two driving actuators and springs for body bending.

II. MECHANICHAL DESIGN

Our developed robot consists of four links and they are connected by three spring joints. Fig. 2 shows a cross-sectional view of a half of the robot and Table II shows its specification. The front rolling and driving units are symmetric with the rear rolling and driving units, respectively. The outputs of the driving and rolling motors were both reduced by the gearhead (the reduction ratio of both were 231:1). Since norminal torque of the driving motor is 15.4mNm, it can theoretically generate approximately 3.5Nm (7.0Nm when two driving wheels are coupled). Due to this high reduction, the hemispherical wheels do not rotate around the roll-axis by reaction forces when moving along the pipe axis. Furthermore, the robot does not fall in the vertical pipe. The angle of the rolling motor can be adjusted by an absolute encoder attached to the rear of the motor.

We assume that this robot is used in dust-, water-, and steam-filled pipes. Each motor is completely sealed by V-rings, O-rings, and rubber sheets to protect the motor from water and dust. Power and communication cables could pass through the inside of the robot through the holes of the joints. Therefore, even when the joints contract and extend, the cables are not tensioned or warped.

The rotational axes of the robot are illustrated in Fig. 3. Only two omni wheels are active in the translational direction along the pipe axis. Conversely, two spherical wheels are active in the rotational direction around the pipe axis. The middle omni wheel is passive in any direction.

Torsion springs are installed in all three joints to shape zigzag movements. Eight holes were arranged in the joint to fix the torsion spring with intervals of 45deg to change the natural angle of the spring.

III. STATIC ANALYSIS FOR DESIGNING SPRING

As shown in Fig. 3, the joints of the robot are contracted by the torsion springs. Despite the actuators generating sufficient propulsive forces against the robot's own weight, the wheels slip if clamping force of the springs is insufficient. Hence, we have derived the driving forces required to move the robot

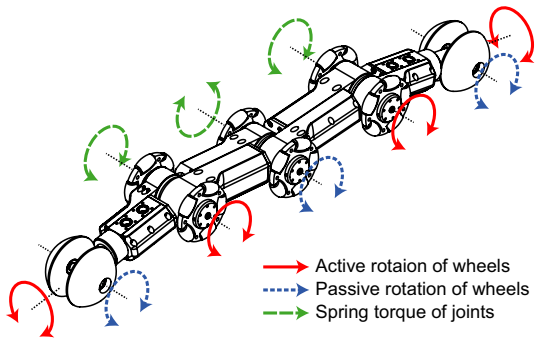

Fig. 3. Rotational axes of the AIRo-Ⅱ

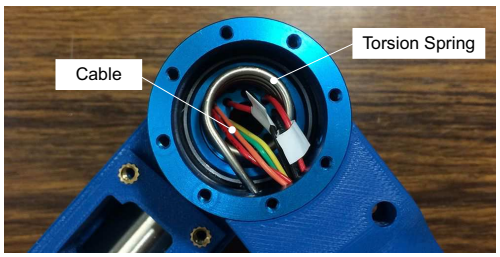

Fig. 4. Joints of the AIRo-Ⅱ

in the vertical pipes. We have also obtained the conditions of the springs to prevent slipping.

A. Kinematic constraints

The multilink-articulated wheeled robot was assumed to be a redundant manipulator as it shared a basic structural similarity [17]. Fig. 5 represents a kinematic model of a non-fixed base 4-link manipulator. L_i, L_{gi}, θ_i, $\boldsymbol{p_i} = \begin{bmatrix} x_i & y_i \end{bmatrix}^T$ and $\boldsymbol{p_{gi}} = \begin{bmatrix} x_{gi} & y_{gi} \end{bmatrix}^T$ are parameters of the i-th link, which denote the link length, length from the former joint to the center of gravity (COG), relative angle of the link, position vector of the joint, and position vector of the COG, respectively. Normally, a 4-link manipulator has four degrees of freedom. However, the base of the robot is not fixed (it floats in the space). In addition to the 4-DOF, other

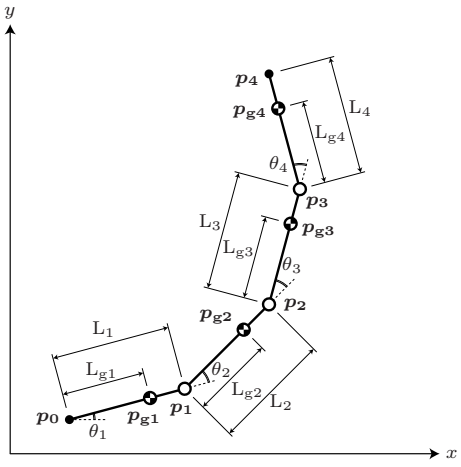

Fig. 5. Kinematic model of a non-fixed base 4-link manipulator

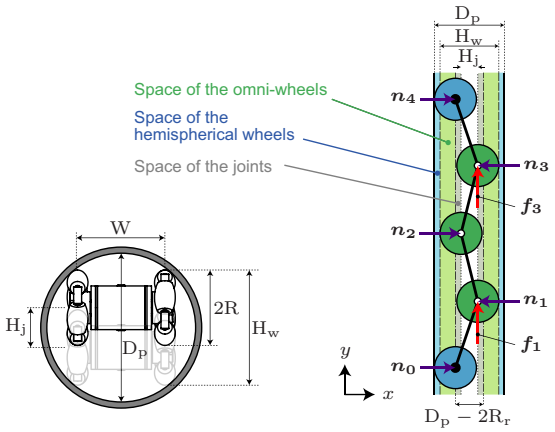

Fig. 6. Restricted space and external forces in a straight pipe

translational motions of the base in x and y directions involve the motion of the whole robot as a variable of $\boldsymbol{p_0}$.

1) Constraint in a straight pipe: Hemispherical wheels (wheels at the head and tail of the robot) can move within the pipe diameter (D_p) as depicted in Fig. 6. In other words, the wheel axes at the head and tail of the robot are restricted within $D_p - 2R$ (R is radius of the wheel). Omni wheels move within the space (H_w) as depicted in Fig. 6. Accordingly, the axes of the omni-wheels are restricted within H_j. From a geometrical relation, H_w and H_j could be obtained by

$$H_w = \sqrt{D_p^2 - W^2} \tag{1}$$

$$H_j = H_w - 2R \tag{2}$$

where W denotes the width between a pair of the omni wheels.

In practice, the force from the inner wall of the pipe is applied to the wheel. Nevertheless, it is assumed that the force applied to the wheel directly transmits to the position of the joint as illustrated in Fig. 6. The angle of each joint when the robot is clamped and statically balanced in the straight pipe can be geometrically calculated by

$$\theta_1 = \cos^{-1} \frac{D_p - 2R_r + H_j}{2L_1} \tag{3}$$

$$\theta_2 = \cos^{-1} \frac{-H_j}{L_2} - \theta_1 \tag{4}$$

$$\theta_3 = \cos^{-1} \frac{H_j}{L_3} - \theta_1 - \theta_2 \tag{5}$$

$$\theta_4 = \cos^{-1} \frac{-(D_p - 2R_r + H_j)}{2L_4} - \theta_1 - \theta_2 - \theta_3 \tag{6}$$

where R_r denote radius of the hemispherical wheel.

2) Constraint in a bent pipe: The multilink-articulated wheeled robot could passively adapt to a corner of the bent pipe owing of its spring joints. However, spring torque decreases while the joint is contracting. As the robot could slip due to the low clamping force, especially in vertical situations, this situation is harder than that of the straight pipe. The clamping force directly relates to the spring torque

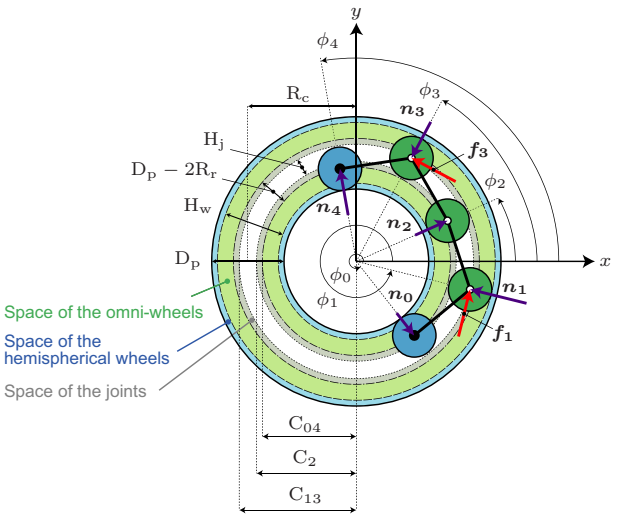

Fig. 7. Restricted space and external forces in a bent pipe

that depends on the stiffness of the spring and the rotational angle from its natural angle.

The amount by which the angle of the joints should shrink in the bent pipe can be geometrically derived as shown in Fig. 7. C_{04}, C_2, and C_{13} all denote the restricted space of the bent pipe, For example, the driving wheels can move within the range from C_2 to C_{13} as well. Each value can be derived by

$$C_{04} = R_c - D_p/2 + R_r \tag{7}$$
$$C_2 = R_c - H_j/2 \tag{8}$$
$$C_{13} = R_c + H_j/2 \tag{9}$$

where R_c denote radius of curvature of the bent pipe.

$\boldsymbol{p_0}$ and $\boldsymbol{p_4}$ must trace a circle of $x^2+y^2 = C_{04}^2$, similarly, $\boldsymbol{p_1}$, $\boldsymbol{p_3}$, and $\boldsymbol{p_2}$ must trace a circle of $x^2+y^2 = C_{13}^2$ and $x^2+y^2 = C_2^2$, respectively. Substituting the position of each joint $\boldsymbol{p_i} = \begin{bmatrix} x_i & y_i \end{bmatrix}^{\mathrm{T}}$ into the above equations of the circles, The angle of the joints could be obtained by

$$\theta_1 = \cos^{-1}\frac{C_{13}^2 - C_{04}^2 - L_1^2}{2L_1C_{04}} + \tan^{-1}\frac{y_0}{x_0} \tag{10}$$
$$\theta_2 = \cos^{-1}\frac{C_2^2 - C_{13}^2 - L_2^2}{2L_2C_{13}} + \tan^{-1}\frac{y_1}{x_1} - \theta_1 \tag{11}$$
$$\theta_3 = \cos^{-1}\frac{C_{13}^2 - C_2^2 - L_3^2}{2L_3C_2} + \tan^{-1}\frac{y_2}{x_2} - \theta_1 - \theta_2 \tag{12}$$
$$\theta_4 = \cos^{-1}\frac{C_{04}^2 - C_{13}^2 - L_4^2}{2L_4C_{13}} + \tan^{-1}\frac{y_3}{x_3} - \theta_1 - \theta_2 - \theta_3 \tag{13}$$

B. Statics of the robot

The equations of force equilibrium could be derived based on the manipulator when the entire body of the robot was clamped in the pipe and statically balanced. The equilibrium of forces must satisfy

$$\boldsymbol{g} + \boldsymbol{n} + \boldsymbol{f} = 0 \tag{14}$$

where $\boldsymbol{g}$, $\boldsymbol{n}$, and $\boldsymbol{f}$ denote gravity force, normal force from inner wall of the pipe, and driving force, respectively, and each vector has two translational dimensions along x and y axes. The equilibrium of moments must satisfy

$$\boldsymbol{m_g} + \boldsymbol{m_n} + \boldsymbol{m_f} + \boldsymbol{m_\tau} = 0 \tag{15}$$

where $\boldsymbol{m_g}$, $\boldsymbol{m_n}$, $\boldsymbol{m_f}$, and $\boldsymbol{m_\tau}$ denote moment of gravity force, moment of normal force, moment of driving force, and torque of the spring, respectively. In this case, there are four links. Thus, each vector has four rotational dimensions of θ_1, θ_2, θ_3, and θ_4.

Since the base of the robot cannot generate torque ($\tau_1 = 0$), the vector of torque is given by

$$\boldsymbol{m_\tau} = \begin{bmatrix} 0 & \tau_2 & \tau_3 & \tau_4 \end{bmatrix}^{\mathrm{T}} \tag{16}$$

Torque of the torsion spring is determined by

$$\tau_i = k(\theta_{\mathrm{nat}i} - \theta_i) \tag{17}$$

where k and θ_{nat} are spring stiffness of the torsion spring and natural angle of the i-th joint, respectively.

1) External forces in a vertical straight pipe: Vector of the normal forces from the inner wall of the pipe and their rotational moments can be defined by

$$\boldsymbol{n} = \boldsymbol{n_0} + \boldsymbol{n_1} + \boldsymbol{n_2} + \boldsymbol{n_3} + \boldsymbol{n_4} \tag{18}$$
$$\boldsymbol{m_n} = \mathbf{J}_1^{\mathrm{T}}\boldsymbol{n_1} + \mathbf{J}_2^{\mathrm{T}}\boldsymbol{n_2} + \mathbf{J}_3^{\mathrm{T}}\boldsymbol{n_3} + \mathbf{J}_4^{\mathrm{T}}\boldsymbol{n_4} \tag{19}$$

and vector of the driving forces and their rotational moments can be also expressed by

$$\boldsymbol{f} = \boldsymbol{f_1} + \boldsymbol{f_3}, \tag{20}$$
$$\boldsymbol{m_f} = \mathbf{J}_1^{\mathrm{T}}\boldsymbol{f_1} + \mathbf{J}_3^{\mathrm{T}}\boldsymbol{f_3} \tag{21}$$

where $\mathbf{J}_i$ denotes the Jacobian matrix of the i-th joint.

As the direction of the normal and driving forces are known, they must be applied in the normal and tangential directions of the inner wall of the pipe, respectively. Therefore, normal forces and driving forces can be described by

$$\boldsymbol{n_i} = n_i\boldsymbol{e_{ni}} \tag{22}$$
$$\boldsymbol{f_i} = f_i\boldsymbol{e_{ti}} \tag{23}$$

where n_i, f_i, $\boldsymbol{e_{ni}}$, and $\boldsymbol{e_{ti}}$ denote the absolute value of the normal force, absolute value of the driving force, unit vectors in normal and tangential directions, respectively.

From the geometrical constraints in a vertical straight pipe, the unit vectors of the forces can be obtained by

$$\boldsymbol{e_{ni}} = \begin{cases} \begin{bmatrix} 1 & 0 \end{bmatrix}^{\mathrm{T}}, & (i = 0, 2, 4) \\ \begin{bmatrix} -1 & 0 \end{bmatrix}^{\mathrm{T}}, & (i = 1, 3) \end{cases} \tag{24}$$
$$\boldsymbol{e_{ti}} = \begin{bmatrix} 0 & 1 \end{bmatrix}^{\mathrm{T}} \tag{25}$$

Here, it is assumed that the velocity of each joint should be 0 because the whole robot body is in equilibrium.

$$\mathbf{A}\dot{\boldsymbol{\theta}} = 0 \tag{26}$$

where $\dot{\boldsymbol{\theta}} = \begin{bmatrix} \dot{\theta}_1 & \dot{\theta}_2 & \dot{\theta}_3 & \dot{\theta}_4 \end{bmatrix}^{\mathrm{T}}$ and $\mathbf{A}$ denotes the 6×4 constraint matrix that can be described by

$$\mathbf{A} = \begin{bmatrix} \boldsymbol{O} \\ \boldsymbol{e}_{\mathbf{n1}}^{\mathbf{T}}\mathbf{J_1} \\ \boldsymbol{e}_{\mathbf{n2}}^{\mathbf{T}}\mathbf{J_2} \\ \boldsymbol{e}_{\mathbf{n3}}^{\mathbf{T}}\mathbf{J_3} \\ \boldsymbol{e}_{\mathbf{n4}}^{\mathbf{T}}\mathbf{J_4} \\ \boldsymbol{e}_{\mathbf{t1}}^{\mathbf{T}}\mathbf{J_1} + \boldsymbol{e}_{\mathbf{t3}}^{\mathbf{T}}\mathbf{J_3} \end{bmatrix} \tag{27}$$

where $\boldsymbol{O} = \begin{bmatrix} 0 & 0 & 0 & 0 \end{bmatrix}$. If the equal driving forces of two wheels are applied as $f = f_1 = f_3$ (same amount of forces are distributed at $\boldsymbol{p_1}$ and $\boldsymbol{p_3}$), Then, the sum of the moments of the normal forces and driving forces are transformed by

$$\boldsymbol{m}_{\mathbf{n}} + \boldsymbol{m}_{\mathbf{f}} = \mathbf{A}^{\mathrm{T}}\boldsymbol{\lambda} \tag{28}$$

where $\boldsymbol{\lambda}$ is a vector of forces which can be expressed by

$$\boldsymbol{\lambda} = \begin{bmatrix} n_0 & n_1 & n_2 & n_3 & n_4 & f \end{bmatrix}^{\mathrm{T}} \tag{29}$$

Substituting (28) into (14) and (15), normal forces and driving forces can be derived by

$$\boldsymbol{\lambda} = -\mathbf{B}^{-1}\left(\begin{bmatrix} \boldsymbol{g} \\ \boldsymbol{m}_{\mathbf{g}} \end{bmatrix} + \begin{bmatrix} 0 \\ \boldsymbol{m}_{\boldsymbol{\tau}} \end{bmatrix}\right) \tag{30}$$

where $\mathbf{B}$ is a 6×6 matrix that can be defined by

$$\mathbf{B} = \begin{bmatrix} \boldsymbol{e}_{\mathbf{n0}} & \boldsymbol{e}_{\mathbf{n1}} & \boldsymbol{e}_{\mathbf{n2}} & \boldsymbol{e}_{\mathbf{n3}} & \boldsymbol{e}_{\mathbf{n4}} & \boldsymbol{e}_{\mathbf{t1}} + \boldsymbol{e}_{\mathbf{t3}} \\ & & & \mathbf{A}^{\mathrm{T}} & & \end{bmatrix} \tag{31}$$

2) External forces in a bent pipe: The unit vectors can be obtained from the geometrical constraints in a bent pipe in a manner similar to the method described above.

$$\boldsymbol{e}_{\mathbf{n}i} = \begin{cases} \begin{bmatrix} \cos\phi_i & \sin\phi_i \end{bmatrix}^{\mathrm{T}} & (i = 0, 2, 4) \\ \begin{bmatrix} \cos(\phi_i + \pi) & \sin(\phi_i + \pi) \end{bmatrix}^{\mathrm{T}} & (i = 1, 3) \end{cases} \tag{32}$$

$$\boldsymbol{e}_{\mathbf{t}i} = \begin{bmatrix} \cos(\phi_i + \pi/2) & \sin(\phi_i + \pi/2) \end{bmatrix}^{\mathrm{T}} \tag{33}$$

This is similar to the process of the vertical straight pipe .

C. Criteria for judging slippage

The driving forces should not exceed the maximum static friction to prevent slippage of the driving wheels Therefore, the driving force f should satisfy both

$$f \leq \mu n_1 \tag{34}$$

$$f \leq \mu n_3 \tag{35}$$

simultaneously, where μ denotes static friction coefficient.

IV. SIMULATION

The parameters used in the simulation were set at the same value as the practical value listed in the Table III. It is widely known that the static friction coefficient can be estimated by $\tan\alpha$ (α: slope angle). From the simple test, urethane material used for the wheels started sliding in a vinyl chloride pipe at approximately $\alpha = 22$deg, and it corresponds to $\mu = 0.4$. Considering nonuniformity of inner surface of the pipe, $\mu = 0.3$ was selected for the simulation.

From (6), when the robot is clamped in the straight pipe, $\theta_2 = 11.6$deg, $\theta_3 = -4.8$deg, and $\theta_4 = 11.6$deg are calculated. On the contrary, from (13), when the robot moves in the bent pipe, $\theta_2 = 68.8$deg, $\theta_3 = 51.7$deg, and $\theta_4 = 68.8$deg are calculated. The natural angle of the joint should satisfy the following in order to generate clamping forces even in the bent pipe, $\theta_{\mathrm{nat}2} < 68.8$deg, $\theta_{\mathrm{nat}4} < 68.8$deg. As the bending direction of joint 3 is opposite to joint 2 and 4, therefore, it should be $\theta_{\mathrm{nat}3} < 0$ and should naturally satisfy $\theta_{\mathrm{nat}3} < 51.7$deg. Therefore, first the natural angle of the joint is set as $\theta_{\mathrm{nat}2} = \theta_{\mathrm{nat}4} = 60$deg and $\theta_{\mathrm{nat}3} = -60$deg.

Basically, an increase in the turns of the torsion spring leads to an increase in the range of movements that the spring can bend in. The maximum possible number of turns becomes 5, based on rest of inner space of the joints. and the diameter of spring wire is also determined as 2mm. In this case, the selectable stiffness of the springs are $k = 0.0025$, 0.0067, and 0.012Nm/deg. In a vertical straight pipe, this spring stiffness determines whether or not the robot slips. Fig. 8 shows the calculation results of the driving force and static friction forces. From the results, only the stiffness where $k = 0.012$Nm/deg satisfies the condition. Hence, this value is selected for designing the torsion spring.

However, the required stiffness to prevent slippage in a bent pipe should be also verified. Fig. 9 (a) and (b) show calculation results of the driving force and static friction forces in a bent pipe, where $\theta_{\mathrm{nat}1} = \theta_{\mathrm{nat}3} = 60$deg & $\theta_{\mathrm{nat}2} = -60$deg and $\theta_{\mathrm{nat}1} = \theta_{\mathrm{nat}3} = 105$deg & $\theta_{\mathrm{nat}2} = -105$deg, respectively.

The robot has anterior-posterior symmetry about the middle omni wheel. Therefore, whether the wheels slip is compared relative to ϕ_2. f_3 exceeds the limitation of the static friction in the range of $0 \leq \phi_2 < 80$deg and 320deg $< \phi_2 < 360$deg as shown in Fig. 9 (a), however, f_1 does not

TABLE III
PARAMETERS OF SIMULATION

Diameter of a pipe ($\mathrm{D_p}$) [m]	0.1
Radius of driving wheels (R) [m]	0.03
Radius of hemispherical wheels ($\mathrm{R_r}$) [m]	0.0325
Radius of curvature of bent pipe ($\mathrm{R_c}$) [m]	0.128
Width between a pair of omni-wheels (W) [m]	0.076
Link length (L_i) [m]	0.125 (i=1, 4), 0.12 (i=2, 3)
Length between end of the link and COG ($\mathrm{L_{g}}_i$) [m]	$\mathrm{L}_i/2$
Static friction coefficient (μ)	0.3
Mass of each link [kg]	0.43

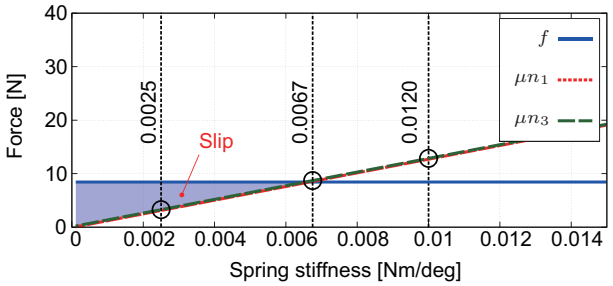

Fig. 8. Selection of spring stiffness: required condition to prevent slippage in a vertical straight pipe

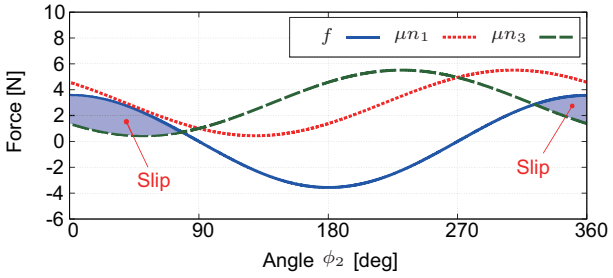

(a) $\theta_{\mathrm{nat1}} = \theta_{\mathrm{nat3}} = 60\mathrm{deg}$ and $\theta_{\mathrm{nat2}} = -60\mathrm{deg}$

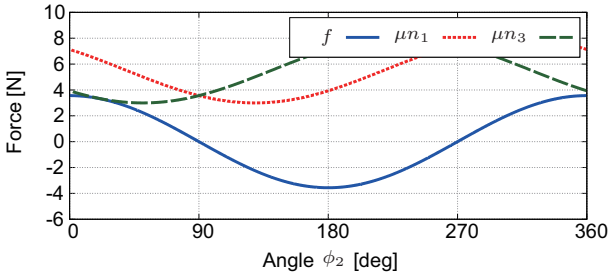

(b) $\theta_{\mathrm{nat1}} = \theta_{\mathrm{nat3}} = 105\mathrm{deg}$ and $\theta_{\mathrm{nat2}} = -105\mathrm{deg}$

Fig. 9. Selection of natural angle of the spring: required condition to prevent slippage in a bent pipe

exceed static friction. This implies that when climbing in a bent pipe, the front driving wheel slips easier than the rear one. By gradually changing the natural angle of the joint, the required value to prevent slippage can be determined as shown in Fig. 9 (b). By summarizing the above, the initial angle of each joint is selected as $\theta_{\mathrm{nat1}} = \theta_{\mathrm{nat3}} = 105\mathrm{deg}$ and $\theta_{\mathrm{nat2}} = -105\mathrm{deg}$.

V. EXPERIMENT

The robot is manually controlled by an operator by using a system as shown in Fig. 10. This is a very simple open loop system that does not involve any servo controller. The right- and left-hand side of the joystick corresponds to the up and down rolling motions and forward and backward movement, respectively.

Experiments are conducted with five trials in a vinyl chloride bent pipe as depicted in Fig. 11. Specifically, the experimental pipe differs from that in the simulation because it is connected by horizontal and vertical straight pipes. However, if the design is based on the simulation, because the joints are more expanded in the experimental

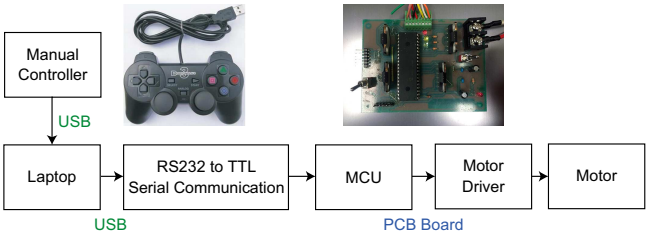

Fig. 10. A system for manual operation

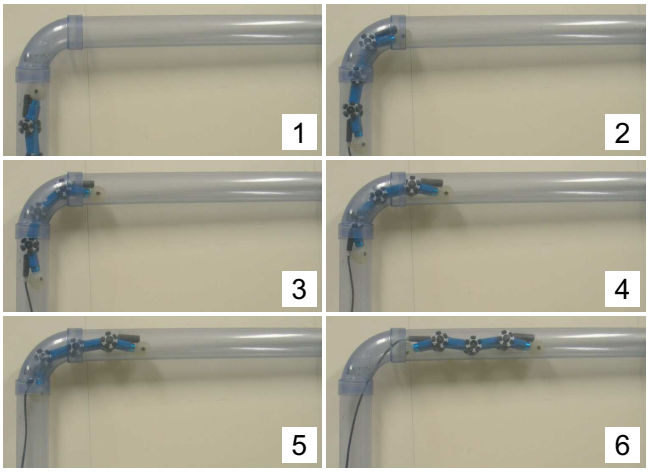

Fig. 11. Experimental result from a vertical straight pipe to a horizontal straight pipe through a bent pipe

setup, it is guaranteed in the experiment as well . Following the simulation results, experiments are conducted with two natural angles of the joints. It was observed that the robot was unable to climb up the bent pipe where $\theta_{\mathrm{nat1}} = \theta_{\mathrm{nat3}} = 60\mathrm{deg}$ and $\theta_{\mathrm{nat2}} = -60\mathrm{deg}$. In contrast, the robot could completely pass through the pipe in all five trials where $\theta_{\mathrm{nat1}} = \theta_{\mathrm{nat3}} = 105\mathrm{deg}$ and $\theta_{\mathrm{nat2}} = -105\mathrm{deg}$. Although, the friction coefficient might not be reliable because the inner wall of the pipe is uneven and curved and as the inertia effect is ignored, The simulation results roughly match with the experimental results. Also, in the situation where a bent pipe connected a horizontal straight pipe to a vertical straight pipe, the robot could climb through it without any slippage even where $\theta_{\mathrm{nat1}} = \theta_{\mathrm{nat3}} = 60\mathrm{deg}$ and $\theta_{\mathrm{nat2}} = -60\mathrm{deg}$.

Furthermore, the experiments were conducted in a flexible winding pipe as shown in Fig. 12. The robot could smoothly pass through a coiling up pipe. It should be noted that because of the omni wheels, the robot can roughly adapt to the pathway without any rolling movement of the hemispherical wheels. Nevertheless, the robot sometimes gets stuck; at this time, rolling movement can recover the robot. More than ten tests were conducted; all trials showed similar results.

To verify the performance, we tested rolling motion in a vertically directed bent pipe (Fig. 13) and turned the robot in a horizontally positioned T-branch in another experiment. Prior to encountering a bent pipe, the initial rolling posture of the robot was set such that the head of the robot is horizontally directed in the side direction. The robot could

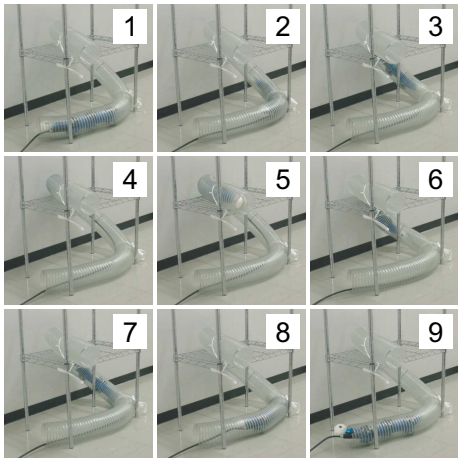

Fig. 12. Experimental result in a winding pipe

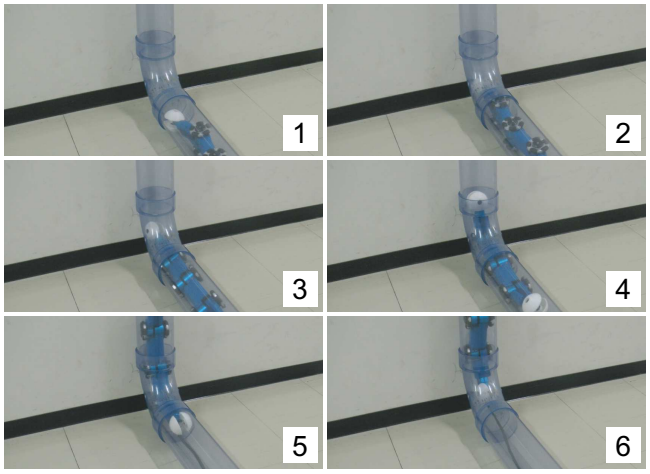

Fig. 13. Rolling motion in a bent pipe

adapt to the pipe by rotating the hemispherical wheels. It could be confirmed that it was successful more than ten times.

At a T-branch, the robot could pass and return to the original position. Two of the five trials were failures because the middle joint bent too much in the T-branch. However, if the robot re-attempts the trial from the start position, then the trial succeeds.

A video of the experiments is uploaded on https://www.youtube.com/watch?v=InEUzUyjRhQ.

VI. CONCLUSIONS

In this paper, we designed a multilink-articulated robot with omni and hemispherical wheels called AIRo-Ⅱ. Only two driving motors were used for this robot due to the limited space. Static analyses in straight pipes and bent pipes are simulated to prevent slippage of the driving wheels within the constraints of number of actuators. These analyses can be used in conjunction with both straight and bent pipes. If the shape of the pipe can be formulated (kinematic constraints are known), the analyses can be used for any pipe shape. Subsequently, the stiffness of the torsion spring and its natural angle are selected.

Lastly, simulation results are verified by experiment. From the experimental results, it was revealed that the robot could adapt to bent, branch, vertical, and winding pipes.

ACKNOWLEDGMENT

This study was supported by Nippon Venture Capital Co., Japan and Program for Creating START-ups from Advanced Research and Technology of The Japan Science and Technology Agency (JST).

REFERENCES

[1] E. Rome, J. Hertzberg, F. Kirchner, U. Licht, and T. Christaller, Towards Autonomous Sewer Robots: the MAKRO Project, Urban Water, vol. 1, pp. 57-70, 1999.

[2] C. Birkenhofer, M. Hoffmeister, J. M. Zollner, R. Dillmann, Compliant Motion of a Multi-segmented Inspection Robot, in Proc. the IEEE/RSJ Int. Conf. Intelligent Robots and Systems, pp. 2632-2637, 2005.

[3] L. Pfotzer, M. Staehler, A. Hermann, A. Roennau, and R. Dillmann, KAIRO 3: Moving Over Stairs & Unknown Obstacles with Reconfigurable Snake-Like Robots, in Proc. the European Conf. Mobile Robots, pp. 1-6, 2015.

[4] H. Schempf, E. Mutschler, A. Gavaert, G. Skoptsov, and W. Crowley, Visual and Nondestructive Evaluation Inspection of Live Gas Mains Using the Explorer^{TM} Family of Pipe Robots, Journal of Field Robotics, vol. 27, pp. 217-249, 2010.

[5] H. M. Kim, Y. S. Choi, H. M. Mun, S. U. Yang, C. M. Park, and H. R. Choi, 2-2D Differential Gear Mechanism for Robot Moving Inside Pipelines, in Proc. the IEEE/RSJ Int. Conf. Intelligent Robots and Systems, pp. 1152-1157, 2015.

[6] H. M. Kim, S. U. Yang, Y. S. Choi, H. M. Mun, C. M. Park, and H. R. Choi, Design of Back-drivable Joint Mechanism for In-pipe Robot, in Proc. the IEEE/RSJ Int. Conf. Intelligent Robots and Systems, pp. 3779-3784, 2015.

[7] E. Dertien, S. Stramigioli, and K. Pulles, Development of an Inspection Robot for Small Diameter Gas Distribution Mains, in Proc. the IEEE Int. Conf. Robotics and Automation, pp. 5044-5049, 2011.

[8] E. Dertien, M. Foumashi, K. Pulles, and S. Stramigioli, Design of a Robot for In-pipe Inspection using Omnidirectional Wheels and Active Stabilization in Proc. the IEEE Int. Conf. Robotics and Automation, pp. 5121-5126, 2014.

[9] K. Isomura and S. Hirose, Development of Articulated Spherical Wheeled In-pipe Robot "ThesV", in Proc. the JSME Conf. Robotics and Mechatronics, pp. 2A2-M02, 2011.

[10] P. Debenest, M. Guarnieri, and S. Hirose, PipeTron Series - Robots for Pipe Inspection, in Proc. the 3rd Int. Conf. Applied Robotics for the Power Industry, pp. 1-6, 2014.

[11] S. Fjerdingen, P. Liljebäck, and A. Transeth, A Snake-like Robot for Internal Inspection of Complex Pipe Structures (PIKo), in Proc. the IEEE/RSJ Int. Conf. Intelligent Robots and Systems, pp. 5665-5671, 2009.

[12] G. C. Vradis and W. Leary, Development of an Inspection Platform and a Suite of Sensors for Assessing Corrosion an Mechanical Damage on Unpiggable Transmission Mains, Technical Report of NGA and Foster-Miller, 2004.

[13] K. Tadakuma, Tetrahedral Mobile Robot with Novel Ball Shape Wheel, in Proc. the First IEEE/RAS-EMBS Int. Conf. Biomedical Robotics and Biomechatronics, pp. 946-952, 2006.

[14] K. Tadakuma, R. Tadakuma, and Jose Berengeres, Development of Holonomic Omnidirectional Vehicle with "Omni-Ball": Spherical Wheels, in Proc. the IEEE/RSJ Int. Conf. Intelligent Robots and Systems, pp. 33-39, 2007.

[15] C. Ye and S. Ma, Development of an Omnidirectional Mobile Platform, In Proc. IEEE Int. Conf. Mechatronics and Automation, pp. 1111-1115, 2009.

[16] A. Kakogawa and S. Ma, An Articulated Wheeled In-pipe Inspection Robot with Holonomic Rolling Motion, in Proc. the Int. Conf. Real-time Computing and Robotics, pp. C2-2, 2015.

[17] S. Ma, Y. Ohmameuda, and K. Inoue, Dynamic Analysis of 3-dimensional Snake Robots, in Proc. the IEEE/RSJ Int. Conf. Intelligent Robots and Systems, pp. 767-772, 2014.